Journal of Colloid and Interface Science 578 (2020) 390–401

Contents lists available at ScienceDirect

Journal of Colloid and Interface Science

journal homepage: www.elsevier.com/locate/jcis

Effect of Ni content in PdNi/C anode catalysts on power and methanol co-generation in alkaline direct methane fuel cell type

M.C.L. Santos [a], C.M. Godoi [a], H.S. Kang [a], R.F.B. de Souza [a], A.S. Ramos [a], E. Antolini [b], A.O. Neto [a,*]

[a] Instituto de Pesquisas Energéticas e Nucleares, IPEN/CNEN-SP, Av. Prof. Lineu Prestes, 2242 Cidade Universitária, CEP 05508-900, São Paulo, SP, Brazil
[b] Scuola di Scienza dei Materiali, Via 25 aprile 22, 16016 Cogoleto, Genova, Italy

GRAPHICAL ABSTRACT

Mass spectroscopy ionic currents (Ii) versus potential values of products obtained from the oxidation of methane at Pd/C, PdNi/C and Ni/C anodes in ADMEFCs.

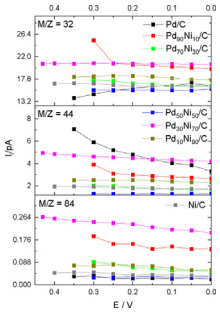

ARTICLE INFO

Article history:
Received 27 April 2020
Revised 2 June 2020
Accepted 4 June 2020
Available online 7 June 2020

Keywords:
Methane
Nickel
Palladium
Alkaline direct methane fuel cell/ADMEFC)
Methanol

ABSTRACT

PdNi electrocatalysts supported on carbon were used as anode materials for methane oxidation in alkaline direct methane fuel cells (ADMEFCs). The electrocatalysts were successfully synthesized by the $NaBH_4$ reduction method. X-ray diffraction measurements showed the formation of non-alloyed Pd in the face- centered cubic (FCC) structure for all materials and formation of NiO and $Ni(OH)_2$ species. TEM images showed that the metal particles are well dispersed on the support with small agglomeration regions. Information about the surface structure of the catalyst were obtained by Raman spectra, mainly confirming the presence of $Ni(OH)_2$. The species observed by DEMS, that is, methanol (m/z = 32), CO_2 (m/z = 44) and potassium formate (m/z = 84) were confirmed by FTIR, which also showed the presence of a high amount of carbonate in the methane oxidation products of the ADMEFC with $Pd_{50}Ni_{50}/C$ as the anode catalyst. Tests in ADMEFCs showed that the dependence of the maximum power density on nickel content in the catalysts goes through a maximum value of 13.5 μW cm^{-2} at 50 at% Ni. Moreover, the amount of produced methanol decreases with increasing Ni content in the PdNi/C catalysts. Both these results can be explained by the enhanced methanol oxidation in the presence of nickel.

1. Introduction

Dependence on fossil fuels warns of environmental awareness arising from the generation of greenhouse gases (GHG) that are a

* Corresponding author.

https://doi.org/10.1016/j.jcis.2020.06.017
0021-9797/

predominant cause of the climate change. However, nowadays do not yet have a source of energy as cheap and comprehensive as they are. In this context, natural gas, composed mainly of methane, used mostly as a source of primary energy, is a powerful greenhouse gas [1].

Thus, the existence of vast reserves of CH_4, low cost and the possibility of transforming it into other more versatile and useful molecules such as methanol, and formate, addressed the research to the conversion of the methane directly into other forms of liquid fuels or higher hydrocarbons of greater added value [1,2]. Several processes for direct methane conversion based on thermal, photo and electrochemical systems, such as catalytic pyrolysis [3,4], oxidative methane coupling [5–7], partial oxidation of methane to methanol and formaldehyde [8] and photocatalysis [9] were previously explored, nevertheless, electrochemical conversion still has the advantage of having as a possible by-product the generation of electric energy [10].

An acceptable selectivity of CH_4 to methanol is achieved only at low/moderate levels of conversion, which results in extensive separation and recycling of unconverted CH_4, since the desired product (intermediate) is much more reactive than the CH_4 itself due to the strong barrier of activation of the C—H bond [11].

The use of methane in fuel cells and its partial oxidation is an alternative way to methane combustion. Methane-fed low temperature fuel cells can be used either to generate only energy (the common use of fuel cells) or to co-generate both energy and methanol. In this context, Proton Exchange Membrane Fuel Cells (PEMFC) could be very interesting, because they operate at relative low temperatures (25–100 °C), with both gas and liquid fuels [12–15]. The use of low molecular weight alcohols as fuels in PEMFCs to generate energy is widely reported in the literature [12,13,15–17]. Thus, PEMFCs fueled with methane could be an appropriate tool to cogeneration of electricity and methanol. First Ferrell et al. [18] evaluated methane oxidation in a PEMFC using a Pt-Ru ELAT anode catalysts, but a poor performance was obtained. Then Joglekar et al. [19] used Pt organometallic complexes supported on ordered mesoporous carbon as anode catalysts in direct methane fuel cells (DMEFCs) operating at 80 °C, obtaining a maximum power density (MPD) of 28 μW cm^{-2}.

Among pure metals, palladium is considered the most promising for methane oxidation at low temperatures, particularly in alkaline media [20,21]. Tests in alkaline direct methane fuel cells (ADMEFCs) showed that pure Pd possess a good selectivity to methanol production, but the power generation is not satisfactory [22]. To increase power generation, a way is the addition of a second metal to Pd. It is known that the addition of Ni to Pd improves methanol oxidation [39–42]. Thus, Ni addition to Pd should increase power generation but at the expense of methanol selectivity. Ni presence, however, could reduce the oxidation of methane to methanol [23–26]. A good compromise between power generation and methanol production should be highly desirable. On these bases, in this work PdNi/C catalysts in different Pd:Ni compositions were used as anode materials in alkaline direct methane fuel cells (ADMEFCs) operating at room temperature and the effect of Ni on the methanol production and cell performance was evaluated.

2. Materials and methods

For preparation of PdNi electrocatalysts in different composition (0, 10, 30, 50, 70, 90 and 100 at% Ni), Palladium Nitrate II ($Pd(NO_3)_2{\cdot}2H_2O$ – Aldrich) and Nickel Chloride II ($NiCl_2{\cdot}6H_2O$ – Aldrich) were used as a source of metals, with a nominal metallic load of 20%, 2-propanol alcohol (Merck) as a solvent, Sodium Borohydride ($NaBH_4$ – Aldrich) as a reducing agent, Potassium Hydroxide (KOH - Merck) and Vulcan® XC72 (Cabot) as a carbon support, under ambient conditions (temperature, pressure and atmosphere). In water/2-propanol 50/50 (*v/v*) solution, the metal precursors and the support were added. Subsequently, 10 mL of 0.01 mol L^{-1} solution of KOH and excess $NaBH_4$ was added. The resulting solution was subjected to stirring for 30 min. The electrocatalysts obtained were vacuum filtered, washed with water and dried at 70 °C for 2 h.

The obtained catalysts were characterized by X-ray diffraction and transmission electron microscopy (TEM). The diffractograms were obtained to have information about the crystalline structure, using the Rigaku diffractometer model Miniflex II with CuKα radiation source (ʎ = 1,54056 Å), scanning in 2Θ from 20° to 90° with a scanning speed of 2°min^{-1}. For TEM experiments were obtained the micrographs in a JEOL Transmission Electron Microscope model JEM-2100 operated at 200 kV, where 150 nanoparticles were digitally measured in each sample to construct the histograms and calculate the average nanoparticle size.

Electrochemical experiments were performed using a three-electrode cell in an Ametek PARSTAT 3000A-DX bipotentiostat/galvanostat. Furthermore, in the conventional electrochemical cell, Ag/AgCl electrode (3 mol L^{-1} KCl) was used as reference electrode and a platinum plate was used as the counter electrode (area = 2 cm^2). On the surface of the working electrode, glassy carbon disc (area = 0.25 cm^2), 15 μl aliquots of each sample of a previously prepared paint composed of a mixture of 8 mg of catalyst + 750 μl of H_2O, 250 μl of isopropyl alcohol and 15 μl of Nafion D-520 at 5%. All experiments with different catalysts were carried out in KOH 1 mol L^{-1} medium.

For ADMEFC tests, the membrane electrode assembly (MEA) was made using a DuPontTM *Nafion*® 117 membrane; two fabrics treated with polytetrafluoroethylene (PTFE – 35%); Pt/C BASF (20% by weight) with 1 mg cm^{-2} as a cathode in the gas diffusion

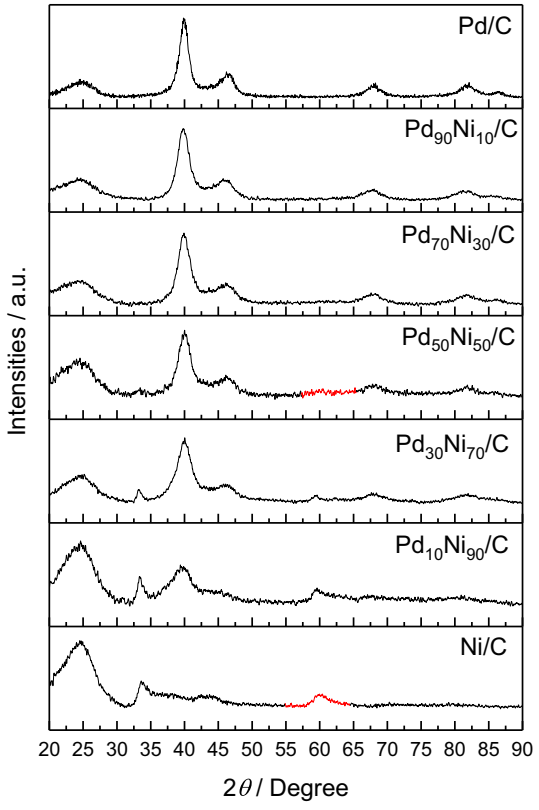

Fig. 1. X-ray diffractograms of PdNi/C electrocatalysts in different atomic compositions.

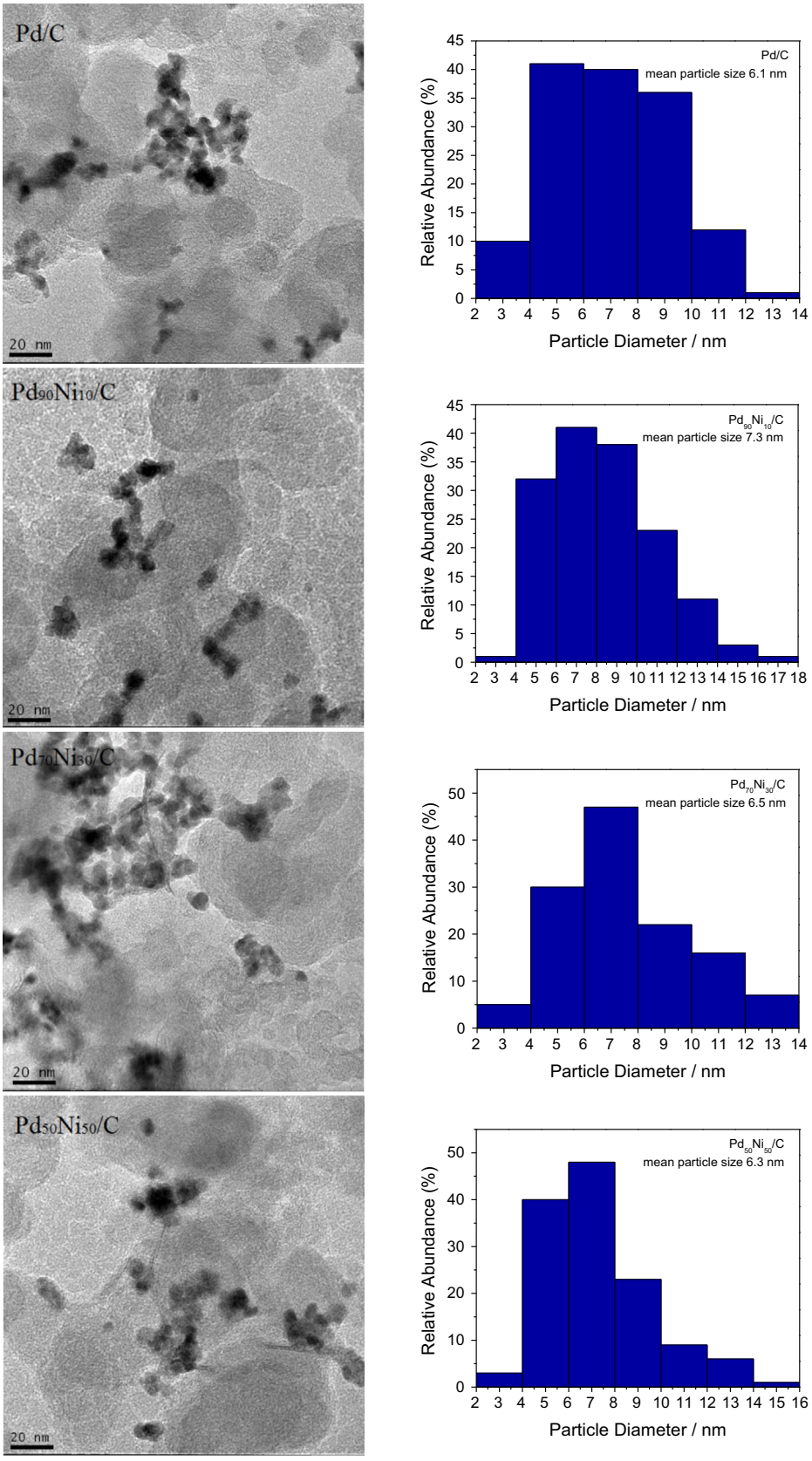

Fig. 2. TEM micrographs and particle size distribution histograms of Pd/C, PdNi/C and Ni/C electrocatalysts.

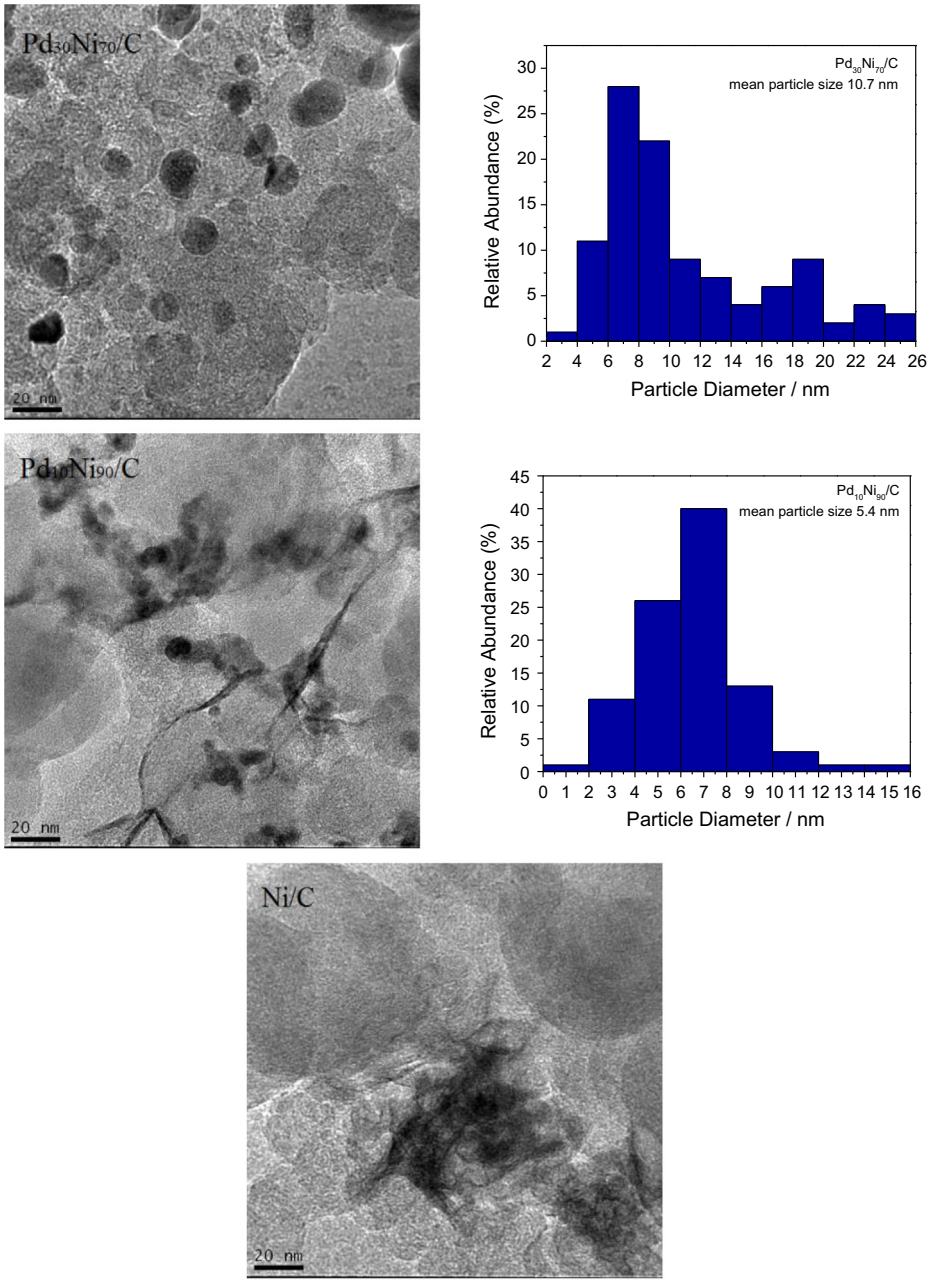

Fig. 2 (*continued*)

electrodes; and catalysts in different proportions of PdNi/C (20% by weight), as an anode. The reactor, a ElectroChem cell with unit-type serpentine distribution, was supplied with CH_4 in a flow of 100 mL min^{-1} and KOH 1.0 mol L^{-1} with a flow of 1 mL min^{-1} at room temperature at the anode and external O_2 with the aid of a humidifier with controlled temperature at 85 °C with a flow of 300 mL min^{-1} in the cathode. The tests were conducted on a specially designed test panel, while the polarization curves were obtained using an Autolab PGSTAT 302 N potentiostat with a current booster.

The ADMEFC measurements were assisted by online differential mass spectroscopy (DMS) coupled to the anode effluent outlet from the reactor. The DMS setup consists of two pumped chambers and a quadrupole mass spectrometer, DaQMS 200 M1, Prisma, Pfeiffer equipped with a continuous dynode secondary electron multiplier/Faraday cup detector having a sensitivity of 200 A $mbar^{-1}$ and 100 a.m.u. mass range. A rotary vane pump (DUO 5, Pfeiffer) was used to pump the primary vacuum chamber and a turbomolecular pump supported by a dry diaphragm pump (hicube 80, Pfeiffer) was used in the secondary chamber. A gas-dosing valve (evn 116, Pfeiffer) connected the two chambers, and the Reactor/DMS interface was sitting on top of the primary vacuum chamber separated by a PTFE membrane (pore size 0.2 μm Whatman®) in continuous flow, and monitored by multiple ion detection by QUADERA® software.

The products obtained from the partial methane oxidation reaction were collected by 180 s increments of 100 mV and analyzed by Fourier Transform Infrared Spectroscopy performed on an ATR accessory (MIRacle with a ZnSe Crystal Plate Pike®) installed on a Nicolet® 6700 FT-IR spectrometer equipped with a cooled MCT

detector with N_2 liquid. The analysis by Raman spectroscopy in this study was used to provide a basis for structural/ qualitative analysis and also for quantitative analysis of products obtained. For the qualitative experiments by Raman spectroscopy, a conventional electrochemical cell was adapted inside MacroRam Raman spectroscopy equipment (Horiba Scientific) to obtain spectra in a wide range of studied potential. And the quantitative analysis of methanol was determined by the method proposed by Boyaci [22,27], using the equipment mentioned. The wavelength was set at 785 nm for all spectra obtained by Raman.

3. Results and discussion

Fig. 1 shown the X-ray diffractograms of Pd/C, PdNi/C and Ni/C electrocatalysts. A peak is observed for all materials at approximately 2θ at 23°, associated with the hexagonal structure of the carbon support equivalent to plane diffraction (1 2 0) (JCPDS # 50–926). For Pd-containing catalysts it is possible to identify peaks at 2θ ≈ 39°, 46°, 68°, 82° and 87° associated, respectively, to the planes (1 1 1), (2 0 0), (2 2 0), (3 1 1) and (2 2 2) of the Pd face-centered cubic (FCC) structure, according to Pd (JCPDS # 89-4897). The absence of shifts of the diffraction peaks of PdNi/C catalysts compared to those of Pd/C indicated no alloy formation. The Ni/C electrocatalyst has two very wide peaks at 37° and 42°, ascribed to NiO (JCPDS # 75-269) and two slight peaks at 34° and 60° associated with the planes (1 0 0) and (1 1 0) of $Ni(OH)_2$ also observed in materials with a high Ni content such as $Pd_{30}Ni_{70}$/C and $Pd_{10}Ni_{90}$/C [28,29].

The micrographs obtained by TEM are illustrated in Fig. 2. The prepared materials present good dispersion with some regions of agglomerations on the carbon support, characteristics inherent to the method employed in this work. The average nanoparticle size values calculated by the particle size distribution histogram are 6.1 nm, 7.3 nm, 6.5 nm, 6.3 nm, 8.5 nm and 5.4 nm for Pd/C, $Pd_{90}Ni_{10}$/C, $Pd_{70}Ni_{30}$/C, $Pd_{50}Ni_{50}$/C, $Pd_{30}Ni_{70}$/C, $Pd_{10}Ni_{90}$/C, respectively. For Ni/C does not possible to evaluate the particle size due to the high agglomeration. The morphology of the materials observed in TEM micrographs with a higher proportion of Ni such as $Pd_{10}Ni_{90}$/C and Ni/C presents an irregular structure that could be related to NiO, this result being consistent with the analysis of XRD and other result described in the literature [30].

The cyclic voltammograms are shown in Fig. 3. The results were obtained from the PdNi/C electrocalysts prepared with different compositions using 1.0 mol L^{-1} KOH solution at room temperature and sweep speed of 10 mV s^{-1}.

All PdNi/C showed the adsorption/desorption peaks not well defined when compared to Pd/C, this behavior validates the presence of Ni in surface, and the process Ni^{2+}/Ni^{3+} is observed at ~−0.1 V in the anodic scan, indicated by the possible formation of nickel oxides [31] and hydroxides [28]. For potentials above −0.4 V an increase in current was observed for the electric double layer region for the $Pd_{30}Ni_{70}$/C electrocatalyst compared to the others. This behavior shows that the addition of Ni to Pd can enhance methane oxidation, as discussed in previous studies [32,33] and it shows that nickel hydroxides ($Ni(OH)_2$ and NiOOH) have high electron and proton conductivity and exhibit high catalytic activity in heterogeneous electrocatalysts.

Fig. 4 shows electrochemical in-situ raman spectra for Pd/C, PdNi/C and Ni/C catalysts in the potential range −0.85 V to 0.15 V, and it is possible to denote the presence of the D and G bands characteristics of graphitic surfaces: the band G (1500 to 1600 cm^{-1}) is attributed to stretching of the C—C bond in graphitic materials and is common to all sp^2 carbon systems, while the D

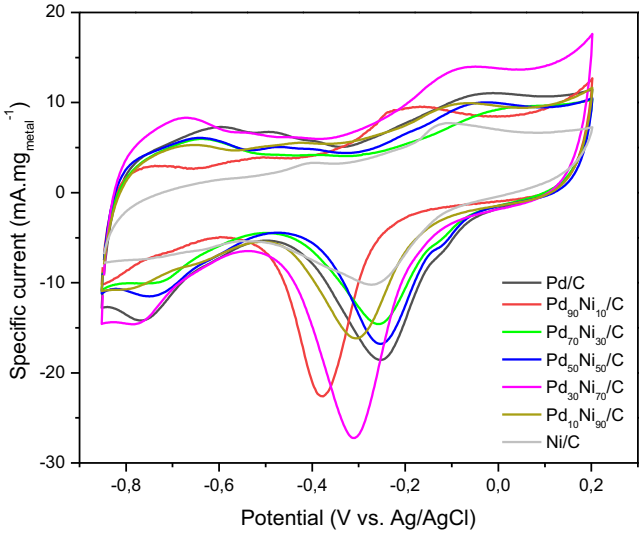

Fig. 3. Voltammograms for Pd/C, $Pd_{90}Ni_{10}$/C, $Pd_{70}Ni_{30}$/C, $Pd_{50}Ni_{50}$/C, $Pd_{30}Ni_{70}$/C, $Pd_{10}Ni_{90}$/C and Ni/C electrocatalysts obtained at a speed of 10 mV s^{-1}, in the presence of 1.0 mol . KOH L^{-1}.

(1200 to 1400 cm^{-1}) and D '(1600 and 1630 cm^{-1}) bands are due to the breathing modes of the sp^2 atoms in rings [34,35].

The G and D bands are present in all materials in a wide potential range. For the Pd/C and $Pd_{90}Ni_{10}$/C electrocatalysts, the G band showed a higher intensity, due to the intense metal-carbon interactions, which suggests that the Pd atoms can be found not only in nanocrystalline clusters, but also in the vicinity of carbon atoms [36]. In addition, in Pd-rich elctrocatalysts the spectrum shows a peak with a position at ≈639 cm^{-1} attributed to the characteristic PdO signal, with little change of intensity from the initial to the final potential [37]. It is also possible to observe in all spectra the band at 794 cm^{-1} that can be attributed to ν (C—S) of *Nafion*® [38].

The characteristic bands for the NiO compound are visible at 497 and 455 cm^{-1}, due to the Ni-O and Ni-OH vibrations, respectively. The $Ni(OH)_2$ compound dehydrates more easily in anodic potentials, so the surface becomes unstable due to the dehydration-hydration reaction, resulting in the growth and decline of the two bands, sometimes in a disordered way [37,39].

Ni possesses a considerable activity for alcohol oxidation in alkaline media. In contact with an alkaline solution nickel becomes covered with a layer of nickel hydroxide, and the surface change can be written as [40,41]

$$Ni + OH^- \rightarrow Ni - OH_{ads} + e^- \quad (1)$$

$$Ni - OH_{ads} \rightarrow (OH - Ni) \quad (2)$$

$$(OH - Ni) + OH^- \rightarrow Ni(OH)_{2,ads} + e^- \quad (3)$$

$$Ni(OH)_2 + OH^- \rightarrow NiOOH + H_2O + e^- \quad (4)$$

The oxidation state of the nickel in the oxide layer likely changes continuously between two and three over a range of potentials. The oxidation of methanol at Ni/NiOOH electrodes in alkaline medium leads to the formation of formate:

$$CH_3OH + NiOOH + OH^- \rightarrow HCOO + Ni(OH)_2 + H_2O \quad (5)$$

Fig. 5 shows the polarization curves for KOH 1.0 mol L^{-1} with a flow of 100 mL min^{-1} of humidified CH_4 for PdNi electrocatalysts in different proportions used as an anode in an ADMEFC operated

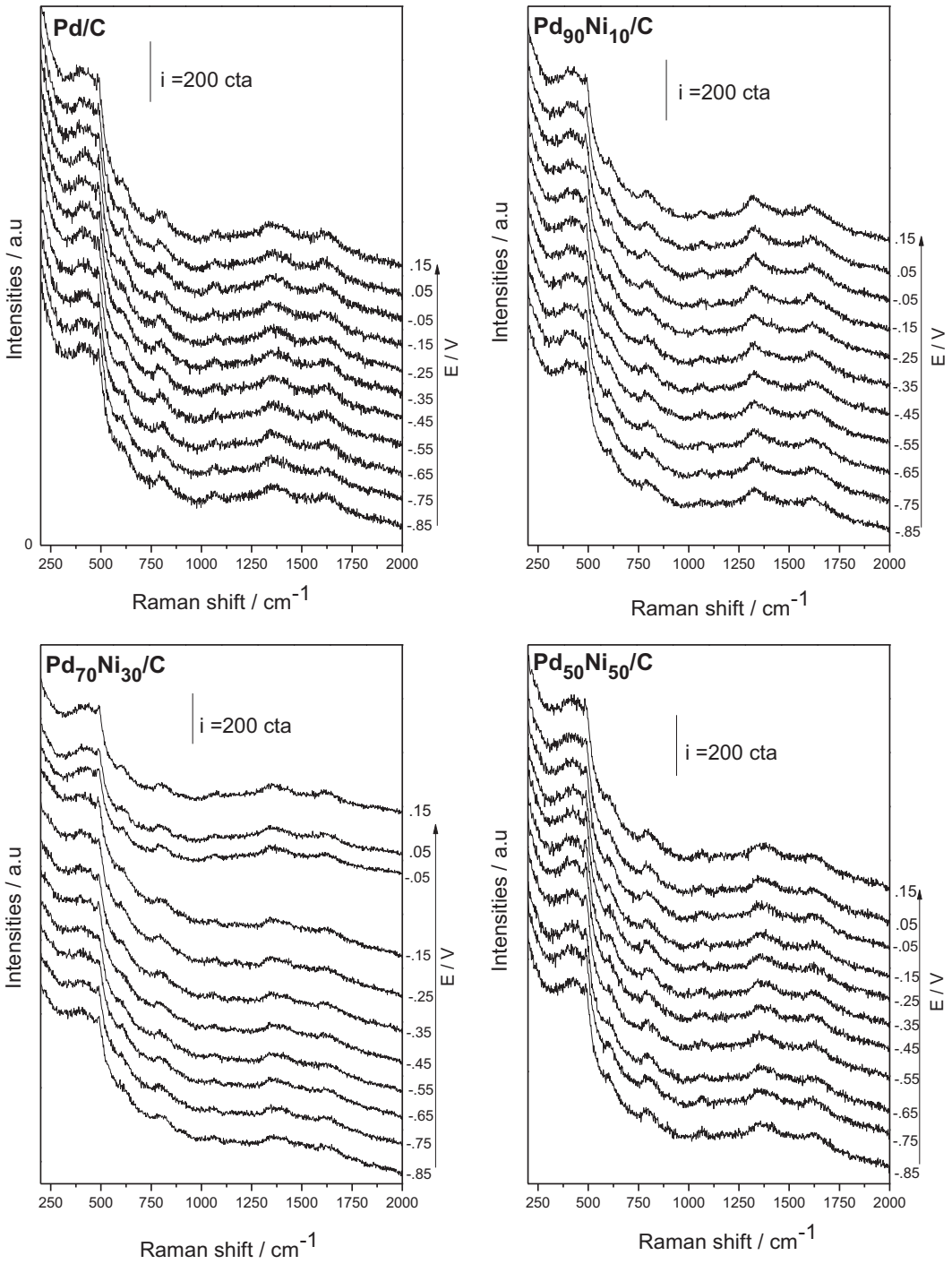

Fig. 4. Raman spectra *in situ* of Pd/C, $Pd_{90}Ni_{10}$/C, $Pd_{70}Ni_{30}$/C, $Pd_{50}Ni_{50}$/C, $Pd_{30}Ni_{70}$/C, $Pd_{10}Ni_{90}$/C and Ni/C electrocatalysts in a 1.0 mol. KOH L^{-1} + flow of 100 mL min^{-1} of CH_4 for 30 min^{-1} at different potentials corresponding to cyclic voltammograms from −0.85 to 0.15 V.

at room temperature. The OCV values obtained (about 0.3 V−0.4 V) are close to those reported by Nandenha [42,43] in a PEMFC and Lee [44] during the galvanic polarization measurements in their fuel cell type reactor. The dependence of the maximum power density (MPD), calculated from the polarization curves in Fig. 5, on Ni content in the catalysts is shown in Fig. 6. The value of MPD goes through a maximum value of 13.5 μW cm^{-2} at 50 at% Ni. The increase of ADMEFC performance in the presence of Ni could be due either to an improved methane conversion or to an enhanced methanol oxidation or both. On the basis of the results of previous works on alkaline direct methanol fuel cells with non-alloyed PdNi/C as the anode catalyst [45–48], that reported an increased methanol oxidation in the presence of NiO, we can suppose that the better performance of Pd-Ni/C catalysts than Pd/C is overall

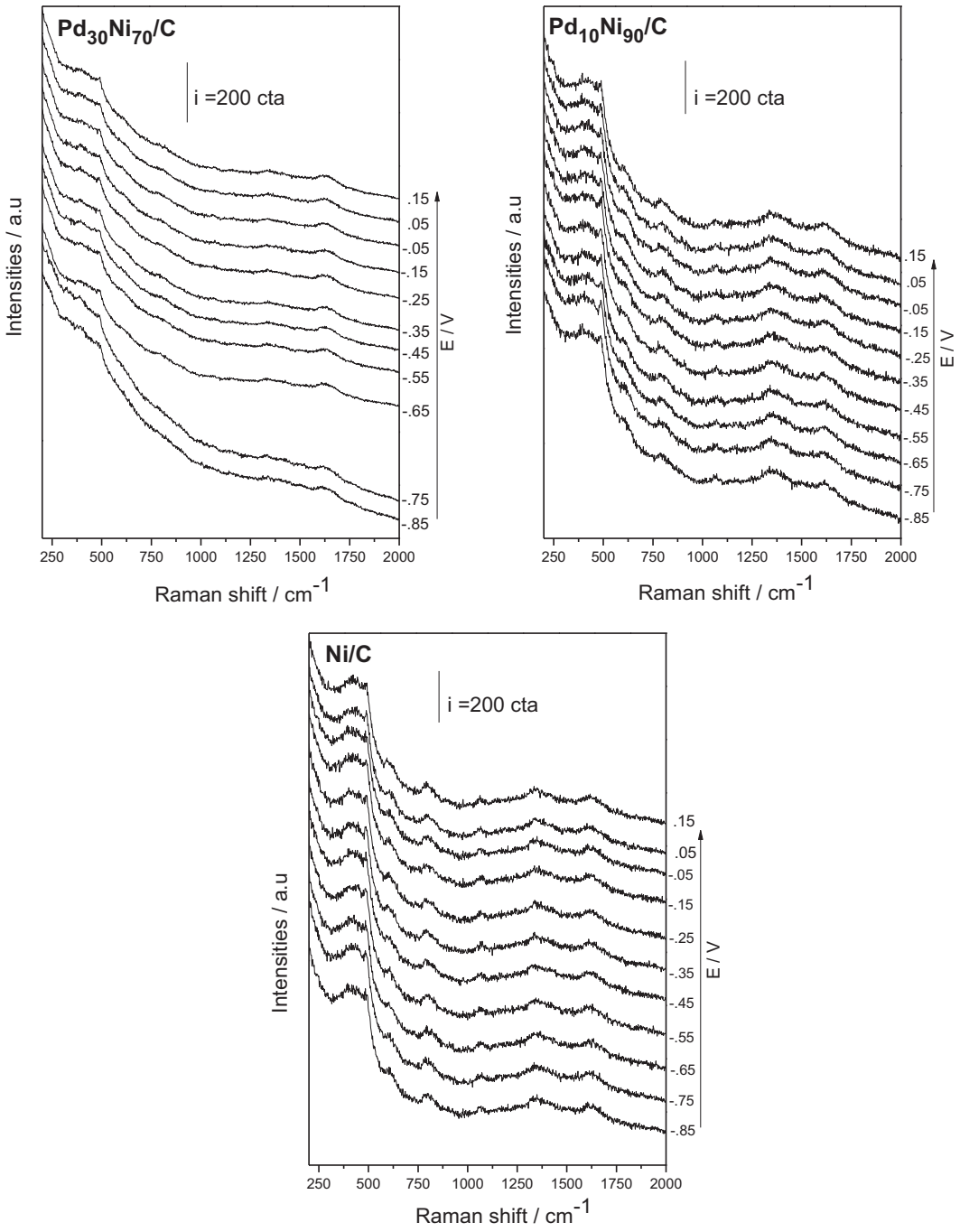

Fig. 4 (*continued*)

due to an enhanced methanol oxidation. The improvement of the activity for methanol oxidation of Pd by Ni addition can be due to the direct methanol oxidation by NiOOH (eq. (5)), to methanol dehydration by NiO, and to the promotion of the formation of PdO active species. The decrease of the MPD for high Ni content in due to the decrease of Pd active sites.

The ADMEFC effluents were analyzed by an online differential electrochemical mass spectrometer (DEMS) at constant flow. In Fig. 7 the ionic currents of the m/z = 32, 44 and 84 ratios are presented corresponding to methanol, carbon dioxide and formate, respectively.

The ionic currents (I_i) to the signal m/z = 32, attributed to methanol, presents an increase observed in the range of potentials close to the OCV for all materials except that the Pd/C material. Between 0.15 V and 0 V, the I_i slightly decreases. This decrease may be linked to the consumption of alcohol produced in ADMEFC,

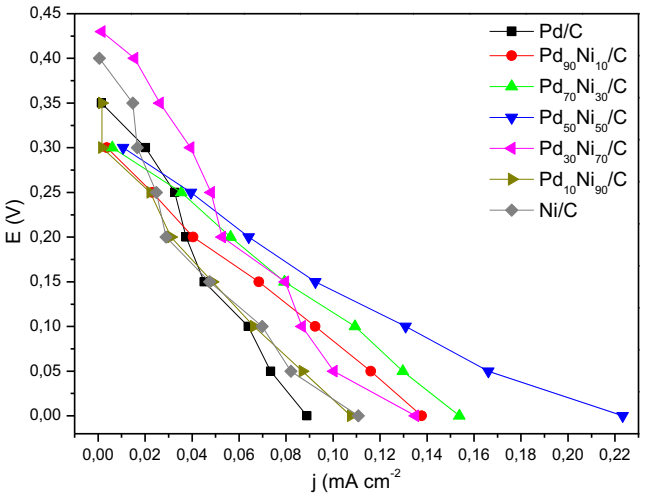

Fig. 5. Polarization curves of PEMFC at room temperature using PdNi/C catalyst anodes in different proportions (1 mg metal^{-2} catalyst loading) and Pt/C BASF for the cathode in all experiments (1 mgPt cm^{-2} of catalyst loading with 20% Pt by weight of carbon), treated Nafion 117 membrane, KOH 1.0 mol L^{-1} + CH_4 100 mL min^{-1} and 300 mL O_2 flow min^{-1}.

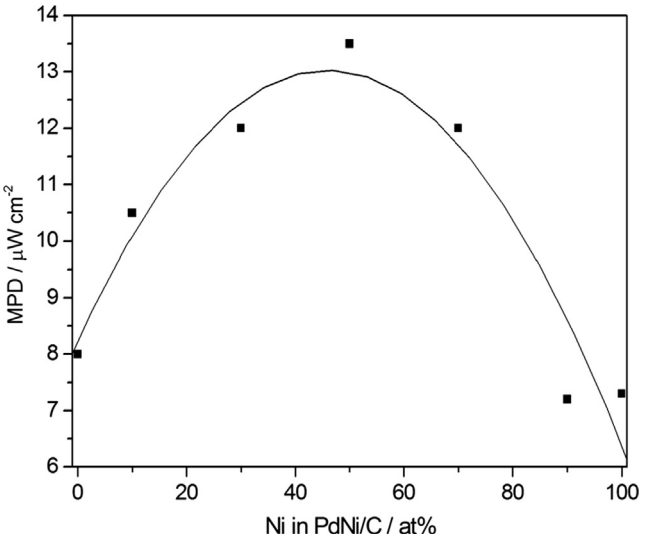

Fig. 6. Dependence of the maximum power density (MPD) of ADMEFCs with PdNi/C anode catalysts on Ni content in the catalysts.

as mentioned in the literature [22,49] in this potential range. The CO_2 evidenced by the signal with m/z = 44, shows an I_i with an abrupt drop of signal for the entire potential range for Pd/C and for the OCV region between 0.30 V and 0.25 V, which shows that there was no complete oxidation of CH_4. For the other materials, an almost linear drop is seen in the entire range of potential, indicating less production of the corresponding species. The signal in m/z = 84 corresponding to the potassium formate, shows a slight decrease from the OCV to 0 V indicating low production for most of the materials.

The DEMS shows the profile of the species due to the partial oxidation of methane; however, in many cases, the I_i can be associated with more than one chemical species. Therefore, ADMEFC effluent samples were analyzed by FTIR to confirm the species obtained.

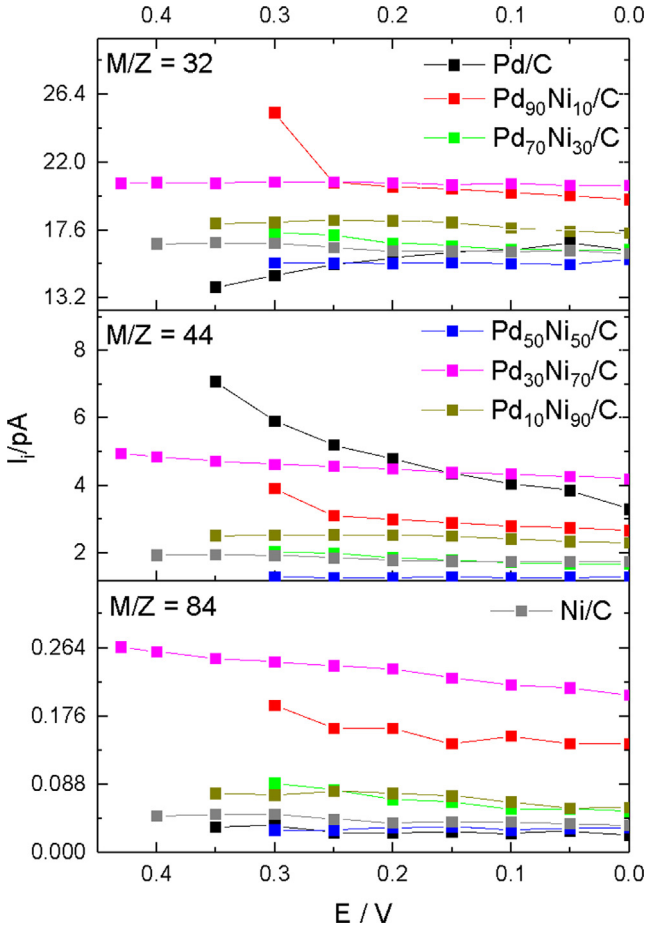

Fig. 7. Mass spectroscopy ionic currents (Ii) versus potential values of products obtained from the oxidation of methane at Pd/C, PdNi/C and Ni/C anodes in ADMEFCs.

Fig. 8 presents the IR spectra of partial oxidation of methane in a ADMEFC. With decreasing potential it is possible to observe an increase of the intensity of the band at ~1302 cm^{-1}, corresponding to the deformation of methane [43,50]. This behavior can be seen in the patterns of Pd/C, $Pd_{90}Ni_{10}$/C and Ni/C and it can be explained by the high solubility of methane in the aqueous KOH solution [51].

Methanol formation is evidenced by bands of 1033, 1077 and 1082 cm^{-1} [52]. The bands at 1033, 1077 cm^{-1} are visible in the $Pd_{70}Ni_{30}$/C pattern almost uniformly over a wide range of potential, and in the $Pd_{50}Ni_{50}$/C pattern between the potentials 0.25 to 0.15 V. The band at 1082 cm^{-1} is visible in the $Pd_{10}Ni_{90}$/C pattern and increases with the potential drop to 0 V. for Ni/C the peak at 1033 cm^{-1} appears in potentials from 0.40 V to 0.30 V and decreases with decreasing potential.

The bands centered at 1342, 1343, 1346 and 1347 cm^{-1}, correspond to the ν(COO) of the formate in the solution [53], are visible in the patterns of the Pd/C, $Pd_{70}Ni_{30}$/C, $Pd_{30}Ni_{70}$/C and Ni/C electrocatalysts. Differently from that observed for the other materials, the $Pd_{50}Ni_{50}$/C electrocatalyst presents good resolution of the carbonate bands (1382 cm^{-1}) in any potential, with greater widening of the band in potentials close to 0 V. The peak instability behavior at different potentials can be explained by the interaction gener-

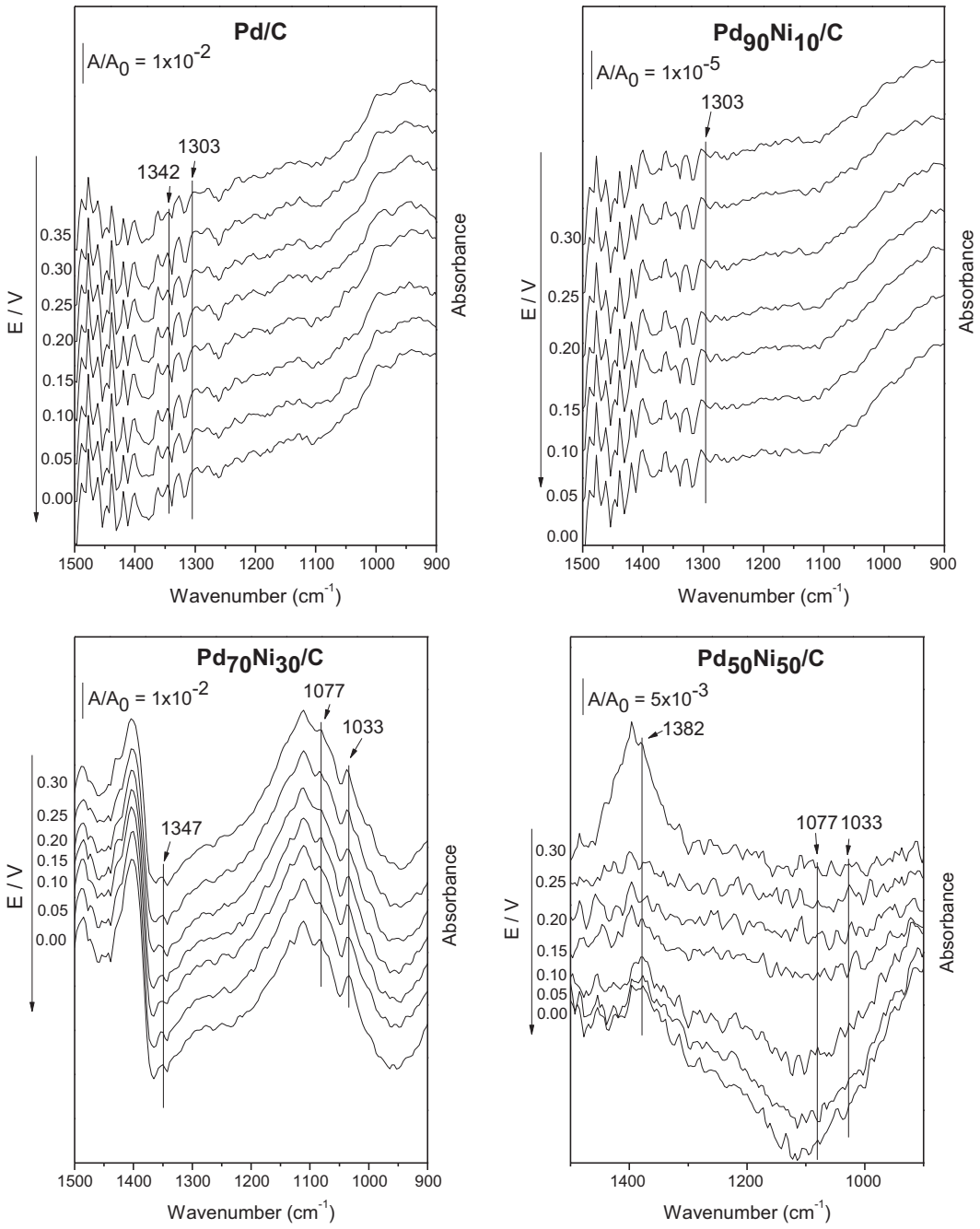

Fig. 8. FTIR spectra *in situ* collected at different potentials in KOH 1.0 mol L^{-1} with methane flow adjusted to 100 mL min^{-1} for all catalysts.

ated by methyl radical with water activated species, as in photocatalytic processes [54–56] and electrochemical oxidative processes [56–58].

The rate of methanol production (r) in the ADMEFC can be quantified by the method of Boyaci [27] adapted by Santos et al. [22]. Fig. 9 illustrates the amount of methanol concentration as a function of the potential that was collected using an analytical curve built in the concentration range of 0.005–1,000 mol L^{-1} of methanol, at the obtained intensity = 4.249 + 4.037 [CH_3OH] with a correlation coefficient of 0.962.

As can be seen in Fig. 9, for each PdNi/C catalyst the maximum rate of methanol production (r_m) is attained at different potentials. The dependence of r_m on Ni content is shown in Fig. 10. An almost linear decrease of r_m with increasing nickel content in the catalysts can be observed in Fig. 10. As in the case of the improvement of the cell performance, and supporting this assumption, also this result should be ascribed to the enhanced methanol oxidation in the nickel presence.

The addition of Ni to Pd decreases the maximum conversion of methane to methanol, however Ni presence promotes methanol oxidation, resulting in an increase of power generation. the Pd_{50}-Ni_{50}/C catalyst showed the highest MPD, due to the complete oxidation of a high amount of methanol to carbonate, as evidenced by FTIR measurements.

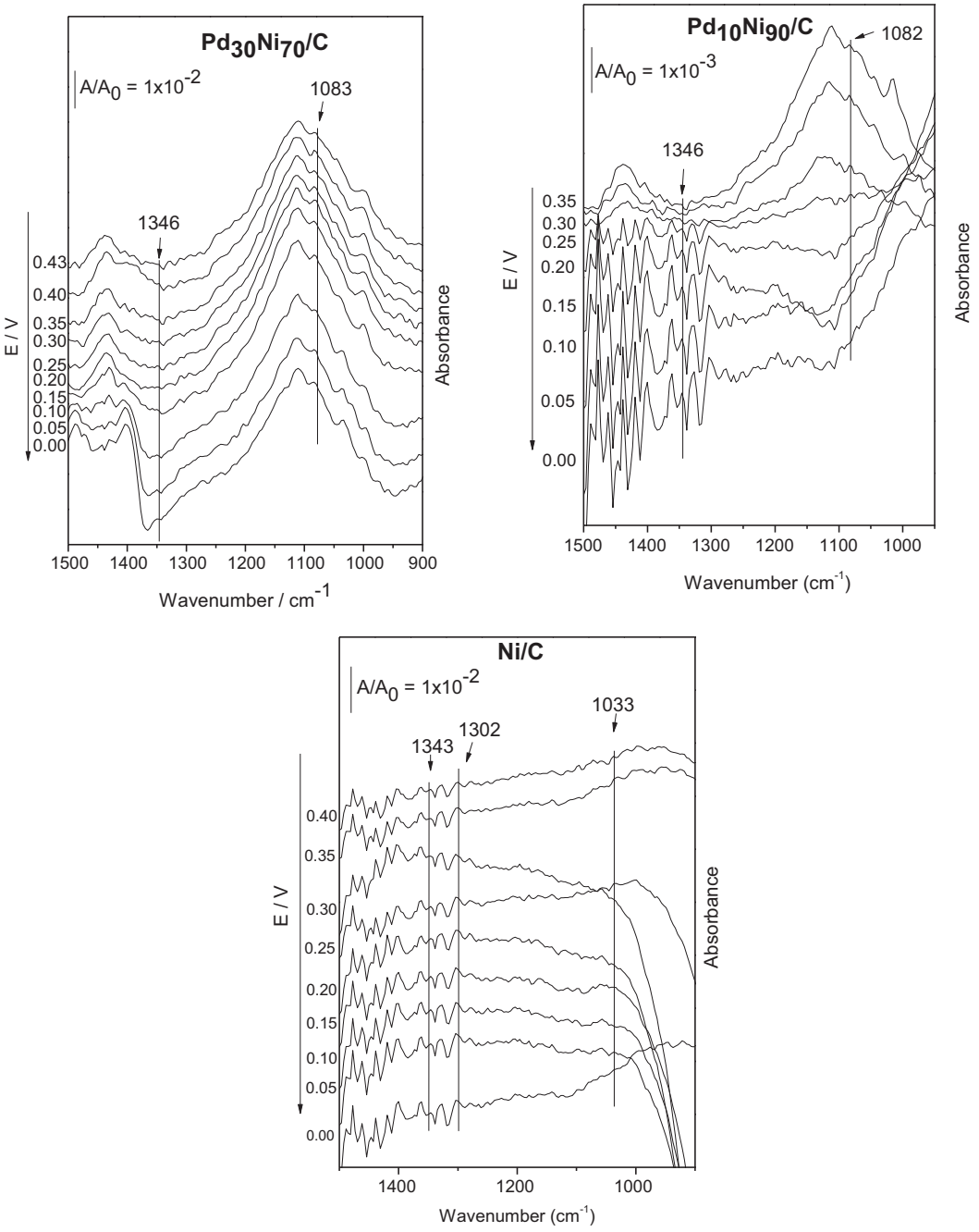

Fig. 8 (*continued*)

4. Conclusion

The effect of Ni content in PdNi/C catalysts used as ADMEFC anode materials on the cell performance and methanol selectivity has been investigated. Characterization techniques such as X-Ray Diffraction, TEM and Raman Spectroscopy, indicated no PdNi alloy formation and differences in the catalytic surface structure associated with the formation of PdO, NiO and Ni $(OH)_2$ compound. Nickel presence enhances the performance of ADMEFCs, by increasing methanol oxidation. The dependence of the MPD on Ni content in the PdNi/C catalysts goes through a maximum. The $Pd_{50}Ni_{50}$/C catalyst showed the highest MPD, due to the complete oxidation of a high amount of methanol to carbonate, as evidenced by FTIR measurements. A monotonous decrease of methanol production with increasing Ni content was observed. .

Summarizing, the use of bare Pd/C as anode catalyst in ADMEFC maximizes methanol production, while the use of PdNi/C in the atomic ratio 1:1 maximizes power generation. A good compromise between power generation and methanol formation could be obtained for a Ni content of 30 at%: at 70 at% Pd the MPD increases by 50%, while methanol production decreases by only 25%.

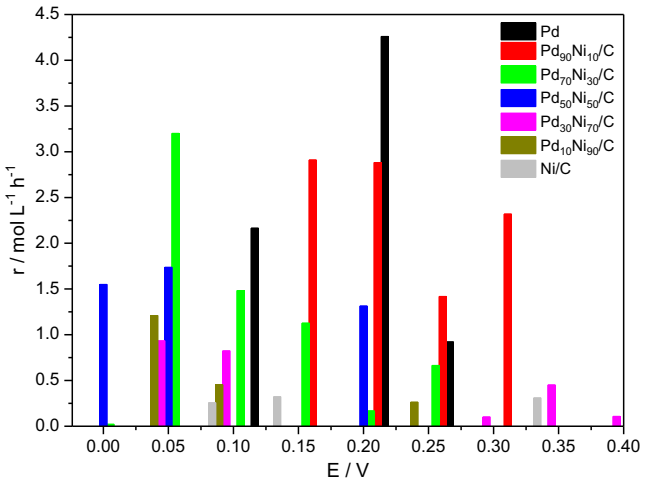

Fig. 9. Rate of methanol production (r) in function of potential in mol $L^{-1}h^{-1}$.

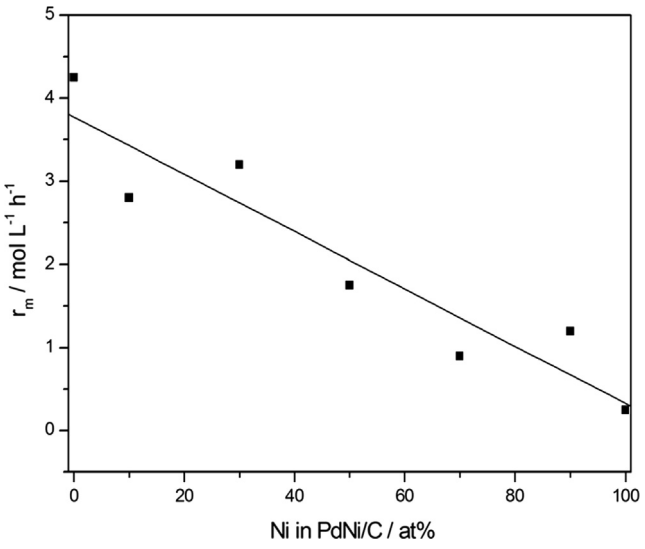

Fig. 10. Dependence of the maximum rate of methanol production (r_m) on nickel content in PdNi/C catalysts.

Declaration of Competing Interest

The authors declare that they have no known competing financial interests or personal relationships that could have appeared to influence the work reported in this paper.

Acknowledgments

We are grateful to CAPES, CNPq (300816/2016-2), FAPESP (2014/09087-4, 2014/50279-4 and 2017/11937-4) and CINE-SHELL (ANP) for financial supports.

Appendix A. Supplementary data

Supplementary data to this article can be found online at https://doi.org/10.1016/j.jcis.2020.06.017.

References

[1] M. Usman, W.W. Daud, H.F. Abbas, Dry reforming of methane: Influence of process parameters—A review, Renew. Sustain. Energy Rev. 45 (2015) 710–744.
[2] M.J. Brown, N.D. Parkyns, Progress in the partial oxidation of methane to methanol and formaldehyde, Catal. Today 8 (3) (1991) 305–335.
[3] A. Holmen, O. Olsvik, O.A. Rokstad, Pyrolysis of natural gas: chemistry and process concepts, Fuel Process. Technol. 42 (2) (1995) 249–267.
[4] L. Wang, L. Tao, M. Xie, G. Xu, J. Huang, Y. Xu, Dehydrogenation and aromatization of methane under non-oxidizing conditions, Catal. Lett. 21 (1) (1993) 35–41.
[5] B. Wang, S. Albarracín-Suazo, Y. Pagán-Torres, E. Nikolla, Advances in methane conversion processes, Catal. Today 285 (2017) 147–158.
[6] G.E. Keller, M.M. Bhasin, Synthesis of ethylene via oxidative coupling of methane: I. Determination of active catalysts, J. Catal. 73 (1) (1982) 9–19.
[7] J.A. Labinger, Methane activation in homogeneous systems, Fuel Process. Technol. 42 (2) (1995) 325–338.
[8] K. Tabata, Y. Teng, T. Takemoto, E. Suzuki, M.A. Bañares, M.A. Peña, J.L.G. Fierro, Activation of methane by oxygen and nitrogen oxides, Catal. Rev. 44 (1) (2002) 1–58.
[9] C.E. Taylor, R.P. Noceti, New developments in the photocatalytic conversion of methane to methanol, Catal. Today 55 (3) (2000) 259–267.
[10] K. Ghaib, F.-Z. Ben-Fares, Power-to-methane: A state-of-the-art review, Renew. Sustain. Energy Rev. 81 (2018) 433–446.
[11] W. Taifan, J. Baltrusaitis, CH4 conversion to value added products: Potential, limitations and extensions of a single step heterogeneous catalysis, Appl. Catal. B 198 (2016) 525–547.
[12] W.J. Zhou, B. Zhou, W.Z. Li, Z.H. Zhou, S.Q. Song, G.Q. Sun, Q. Xin, S. Douvartzides, M. Goula, P. Tsiakaras, Performance comparison of low-temperature direct alcohol fuel cells with different anode catalysts, J. Power Sources 126 (1–2) (2004) 16–22.
[13] F. Munoz, C. Hua, T. Kwong, L. Tran, T.Q. Nguyen, J.L. Haan, Palladium–copper electrocatalyst for the promotion of the electrochemical oxidation of polyalcohol fuels in the alkaline direct alcohol fuel cell, Appl. Catal. B 174–175 (2015) 323–328.
[14] S. Rousseau, C. Coutanceau, C. Lamy, J.M. Léger, Direct ethanol fuel cell (DEFC): Electrical performances and reaction products distribution under operating conditions with different platinum-based anodes, J. Power Sources 158 (1) (2006) 18–24.
[15] M. Shao, Palladium-based electrocatalysts for hydrogen oxidation and oxygen reduction reactions, J. Power Sources 196 (5) (2011) 2433–2444.
[16] A.B. Yousaf, M. Imran, A. Zeb, T. Wen, X. Xie, Y.-F. Jiang, C.-Z. Yuan, A.-W. Xu, Single phase PtAg bimetallic alloy nanoparticles highly dispersed on reduced graphene oxide for electrocatalytic application of methanol oxidation reaction, Electrochim. Acta 197 (2016) 117–125.
[17] X. Chen, T. Li, J. Shen, Z. Hu, From structures, packaging to application: A system-level review for micro direct methanol fuel cell, Renew. Sustain. Energy Rev. 80 (2017) 669–678.
[18] J.R. Ferrell, S. Sachdeva, T.A. Strobel, G. Gopalakrishan, C.A. Koh, G. Pez, A.C. Cooper, A.M. Herring, Exploring the fuel limits of direct oxidation proton exchange membrane fuel cells with platinum based electrocatalysts, J. Electrochem. Soc. 159 (4) (2012) B371–B377.
[19] M. Joglekar, V. Nguyen, S. Pylypenko, C. Ngo, Q. Li, M.E. O'Reilly, T.S. Gray, W.A. Hubbard, T.B. Gunnoe, A.M. Herring, B.G. Trewyn, Organometallic complexes anchored to conductive carbon for electrocatalytic oxidation of methane at low temperature, J. Am. Chem. Soc. 138 (1) (2016) 116–125.
[20] J.H. Lee, D.L. Trimm, Catalytic combustion of methane, Fuel Process. Technol. 42 (2) (1995) 339–359.
[21] Q. Mao, A.C.T. van Duin, K.H. Luo, Investigation of methane oxidation by palladium-based catalyst via ReaxFF Molecular Dynamics simulation, Proc. Combust. Inst. 36 (3) (2017) 4339–4346.
[22] M.C.L. Santos, L.C. Nunes, L.M.G. Silva, A.S. Ramos, F.C. Fonseca, R.F.B. de Souza, A.O. Neto, Direct alkaline anion exchange membrane fuel cell to converting methane into methanol, ChemistrySelect 4 (39) (2019) 11430–11434.
[23] L. Arnarson, P.S. Schmidt, M. Pandey, A. Bagger, K.S. Thygesen, I.E.L. Stephens, J. Rossmeisl, Fundamental limitation of electrocatalytic methane conversion to methanol, PCCP 20 (16) (2018) 11152–11159.
[24] A. Mohsenzadeh, T. Richards, K. Bolton, DFT study of the water gas shift reaction on Ni(111), Ni(100) and Ni(110) surfaces, Surf. Sci. 644 (2016) 53–63.
[25] F. Che, J.T. Gray, S. Ha, J.-S. McEwen, Catalytic water dehydrogenation and formation on nickel: Dual path mechanism in high electric fields, J. Catal. 332 (2015) 187–200.
[26] S. Liu, T. Ishimoto, M. Koyama, First-principles study of oxygen coverage effect on hydrogen oxidation on Ni(111) surface, Appl. Surf. Sci. 333 (2015) 86–91.
[27] I.H. Boyaci, H.E. Genis, B. Guven, U. Tamer, N. Alper, A novel method for quantification of ethanol and methanol in distilled alcoholic beverages using Raman spectroscopy, J. Raman Spectrosc. 43 (8) (2012) 1171–1176.
[28] S.Y. Shen, T.S. Zhao, J.B. Xu, Y.S. Li, Synthesis of PdNi catalysts for the oxidation of ethanol in alkaline direct ethanol fuel cells, J. Power Sources 195 (4) (2010) 1001–1006.
[29] M. Simões, S. Baranton, C. Coutanceau, Electro-oxidation of glycerol at Pd based nano-catalysts for an application in alkaline fuel cells for chemicals and energy cogeneration, Appl. Catal. B 93 (3–4) (2010) 354–362.
[30] X. Guo, A. Traitangwong, M. Hu, C. Zuo, V. Meeyoo, Z. Peng, C. Li, Carbon dioxide methanation over nickel-based catalysts supported on various mesoporous material, Energy Fuels 32 (3) (2018) 3681–3689.
[31] R.S. Amin, R.M. Abdel Hameed, K.M. El-Khatib, M. Elsayed Youssef, Electrocatalytic activity of nanostructured Ni and Pd–Ni on Vulcan XC-72R carbon black for methanol oxidation in alkaline medium, Int. J. Hydrogen Energy 39 (5) (2014) 2026–2041.

[32] J.-H. Choi, K.-W. Park, B.-K. Kwon, Y.-E. Sung, Methanol Oxidation on Pt/Ru, Pt/Ni, and Pt/Ru/Ni Anode Electrocatalysts at Different Temperatures for DMFCs, J. Electrochem. Soc. 150 (7) (2003) A973.
[33] Z.-B. Wang, P.-J. Zuo, G.-J. Wang, C.-Y. Du, G.-P. Yin, Effect of Ni on PtRu/C catalyst performance for ethanol electrooxidation in acidic medium, J. Phys. Chem. C 112 (16) (2008) 6582–6587.
[34] W. Li, H. Zhang, C. Wang, Y. Zhang, L. Xu, K. Zhu, S. Xie, Raman characterization of aligned carbon nanotubes produced by thermal decomposition of hydrocarbon vapor, Appl. Phys. Lett. 70 (20) (1997) 2684–2686.
[35] R.J. Nemanich, S.A. Solin, First- and second-order Raman scattering from finite-size crystals of graphite, Phys. Rev. B 20 (2) (1979) 392–401.
[36] J. Lee, K.S. Novoselov, H.S. Shin, Interaction between Metal and graphene: dependence on the layer number of graphene, ACS Nano 5 (1) (2011) 608–612.
[37] K. Gopalsamy, J. Balamurugan, T.D. Thanh, N.H. Kim, D. Hui, J.H. Lee, Surfactant-free synthesis of NiPd nanoalloy/graphene bifunctional nanocomposite for fuel cell, Compos. B Eng. 114 (2017) 319–327.
[38] V. Di Noto, R. Gliubizzi, E. Negro, M. Vittadello, G. Pace, Hybrid inorganic-organic proton conducting membranes based on Nafion and 5 wt.% of MxOy (M = Ti, Zr, Hf, Ta and W): Part I. Synthesis, properties and vibrational studies, Electrochim. Acta 53 (4) (2007) 1618–1627.
[39] Y.L. Lo, B.J. Hwang, In Situ Raman studies on cathodically deposited nickel hydroxide films and electroless Ni−P electrodes in 1 M KOH solution, Langmuir 14 (4) (1998) 944–950.
[40] M. Alsabet, M. Grden, G. Jerkiewicz, Electrochemical growth of surface oxides on nickel. Part 1: formation of α-Ni(OH)2 in relation to the polarization potential polarization time, and temperature, Electrocatalysis 2 (4) (2011) 317–330.
[41] B.E. Conway, B. Barnett, H. Angerstein-Kozlowska, B.V. Tilak, A surface-electrochemical basis for the direct logarithmic growth law for initial stages of extension of anodic oxide films formed at noble metals, J. Chem. Phys. 93 (11) (1990) 8361–8373.
[42] J. Nandenha, I. Nagahama, J. Yamashita, E. Fontes, J. Ayoub, R. de Souza, F. Fonseca, A. Neto, Activation of Methane on PdZn/C Electrocatalysts in an Acidic Electrolyte at Low Temperatures, Int. J. Electrochem. Sci. 14 (2019) 10819–10834.
[43] J. Nandenha, E.H. Fontes, R.M. Piasentin, F.C. Fonseca, A.O. Neto, Direct oxidation of methane at low temperature using Pt/C, Pd/C, Pt/C-ATO and Pd/C-ATO electrocatalysts prepared by sodium borohydride reduction process, J. Fuel Chem. Technol. 46 (9) (2018) 1137–1145.
[44] B. Lee, T. Hibino, Efficient and selective formation of methanol from methane in a fuel cell-type reactor, J. Catal. 279 (2) (2011) 233–240.
[45] P.K. Shen, C. Xu, R. Zeng, Y. Liu, Electro-oxidation of Methanol on NiO-Promoted Pt / C and Pd / C Catalysts, Electrochem. Solid-State Lett. 9 (2) (2006) A39–A42.
[46] M. Wang, W. Liu, C. Huang, Investigation of PdNiO/C catalyst for methanol electrooxidation, Int. J. Hydrogen Energy 34 (6) (2009) 2758–2764.
[47] K.-H. Ye, S.-A. Zhou, X.-C. Zhu, C.-W. Xu, P.K. Shen, Stability analysis of oxide (CeO2, NiO, Co3O4 and Mn3O4) effect on Pd/C for methanol oxidation in alkaline medium, Electrochim. Acta 90 (2013) 108–111.
[48] Y. Song, X. Zhang, S. Yang, X. Wei, Z. Sun, Electrocatalytic performance for methanol oxidation on nanoporous Pd/NiO composites prepared by one-step dealloying, Fuel 181 (2016) 269–276.
[49] J. Nandenha, R.M. Piasentin, L.M.G. Silva, E.H. Fontes, A.O. Neto, R.F.B. de Souza, Partial oxidation of methane and generation of electricity using a PEMFC, Ionics 25 (10) (2019) 5077–5082.
[50] D. Scarano, S. Bertarione, G. Spoto, A. Zecchina, C. Otero, Areán, FTIR spectroscopy of hydrogen, carbon monoxide, and methane adsorbed and co-adsorbed on zinc oxide, Thin Solid Films 400 (1) (2001) 50–55.
[51] L.-K. Wang, G.-J. Chen, G.-H. Han, X.-Q. Guo, T.-M. Guo, Experimental study on the solubility of natural gas components in water with or without hydrate inhibitor, Fluid Phase Equilib. 207 (1) (2003) 143–154.
[52] K. Hamada, H. Morishita, The Rotation-Vibrational Spectra and Structures of Methanol and Acetonitrile, Spectrosc. Lett. 13 (1) (1980) 15–29.
[53] P.A. Christensen, D. Linares-Moya, The role of adsorbed formate and oxygen in the oxidation of methanol at a polycrystalline Pt electrode in 0.1 M KOH: an in situ fourier transform infrared study, J. Phys. Chem. C 114 (2) (2010) 1094–1101.
[54] Á. López-Martín, A. Caballero, G. Colón, Photochemical methane partial oxidation to methanol assisted by H2O2, J. Photochem. Photobiol., A 349 (2017) 216–223.
[55] S. Sun, Y.-C. Zhang, G. Shen, Y. Wang, X. Liu, Z. Duan, L. Pan, X. Zhang, J.-J. Zou, Photoinduced composite of Pt decorated Ni(OH)2 as strongly synergetic cocatalyst to boost H2O activation for photocatalytic overall water splitting, Appl. Catal. B 243 (2019) 253–261.
[56] X. Zhang, B. Zhang, S. Liu, H. Kang, W. Kong, S. Zhang, Y. Shen, B. Yang, RGO modified Ni doped FeOOH for enhanced electrochemical and photoelectrochemical water oxidation, Appl. Surf. Sci. 436 (2018) 974–980.
[57] R.K. Singh, A. Schechter, Electrochemical investigation of urea oxidation reaction on β Ni(OH)2 and Ni/Ni(OH)2, Electrochim. Acta 278 (2018) 405–411.
[58] X. Shang, B. Dong, Y.-M. Chai, C.-G. Liu, In-situ electrochemical activation designed hybrid electrocatalysts for water electrolysis, Sci. Bull. 63 (13) (2018) 853–876.